IEEE Access
Multidisciplinary | Rapid Review | Open Access Journal

Received October 6, 2019, accepted October 21, 2019, date of publication November 4, 2019, date of current version November 20, 2019.

*Digital Object Identifier 10.1109/ACCESS.2019.2951282*

# Robust and Adaptive Backstepping Control for Hexacopter UAVs

**JUQIAN ZHANG[1], DAWEI GU[1], CHAO DENG[2], AND BANGCHUN WEN[1]**
[1]School of Mechanical Engineering and Automation, Northeastern University, Shenyang 110819, China
[2]School of Electrical and Electronic Engineering, Nanyang Technological University, Singapore 639798

Corresponding author: Juqian Zhang (zhangjuqian@126.com)

This work was supported in part by the National Natural Science Foundation of China under Grant U1708257, Grant 61773056, and Grant 51875093, and in part by the National Key Research and Development Program of China under Grant 2017YFB1103702.

**ABSTRACT** A nonlinear robust and adaptive backstepping control strategy is hierarchically proposed to solve the trajectory tracking problem of hexacopter UAVs. Due to the under-actuated and coupled properties of the hexacopter dynamics, the nominal backstepping control approach is fully designed as the main controller. Considering the model uncertainties and external disturbances perturbing the system stability, a robust $2^{nd}$-order linear extended state observer (LESO) with more reliable velocity feedback is devised to observe and suppress the instabilities, and peaking phenomena in the observation are removed. Usually, large observer gains are selected to reduce the tracking errors but will amplify the measurement noise. To further enhance the system robustness, an adaptive switching function based compensator is introduced to eliminate the observation errors, through which the requirement on large observer gains is relaxed, and high gain behaviors of the LESO are avoided. Stability analysis proves that the nonlinear control scheme can ensure the hexacopter UAV asymptotic tracking along the designated trajectory. Comparative simulations under different controllers are carried out to demonstrate the efficiency and superiority of the proposed control scheme.

**INDEX TERMS** Hexacopter UAV, trajectory tracking, robust backstepping control, $2^{nd}$-order LESO, hierarchical compensators.

## I. INTRODUCTION

In the last decades, the Unmanned Aerial Vehicles (UAVs) have achieved significant development. Various types of UAVs with different structures, favorable performances, and wide applications keep emerging. The multi-rotor UAV has attracted great attention recently because of its prominent advantages in hovering capability, high maneuverability, simple structure, and reduced costs [1]–[3]. The most representative one is the quadrotor UAV, which is widely applied in the aerial photograph, inspection, rescue, cargo transportation, and precision agriculture, *etc.*, [4], [5]. Note that only four rotors are mounted in the quadrotor UAV, and limited power can be provided, which limits its application, especially for cargo delivery. Nowadays, the design of multi-rotor UAV with more rotors (e.g., the hexacopter and octocopter UAV) is fast-growing, and the advantages appear in terms of more lift and more time on the fly [6]–[8]. However, more rotors bring bigger size and higher costs. So the hexacopter UAV appears to be a compromise, and it is most widely used in the specific occasions [9]. Nevertheless, it is still a challenge to design an effective controller ensuring the multi-rotor UAV robust flight capabilities due to following major reasons [10]–[13]: (1) The multi-rotor UAV is a typical under-actuated system with 6-DOF (degree of freedom) but only four control inputs; (2) it is a complicated system with strong nonlinearity and coupling characters, where the translational subsystem dynamics and the rotational one interact on each other; (3) there always exist parameter uncertainties, un-modeled dynamics and external disturbances degrading the system stability and control performances. These problems have attracted special attention from many researchers.

To address the above problems, plentiful control methods have been presented. Initially, some linear control methods, including PID [14], LQR [15], and $H\infty$ control [16] have been adopted for the fundamental flight capabilities of the multi-rotor UAV. However, these linear approaches are sensitive to the nonlinearities, and the flight performance will be

The associate editor coordinating the review of this manuscript and approving it for publication was Mark Kok Yew Ng.

degraded when the disturbances occur. In order to improve the robust control performance, more efforts have been made on the nonlinear control approaches, such as backstepping control [17], sliding mode control (SMC) [18], active disturbance rejection control (ADRC) [19], fuzzy control and other intelligent control methods [20]–[22]. The SMC method is insensitive to the disturbances and is widely applied for the nonlinear systems [23], [24]. However, the chattering phenomenon always exists in the control system and brings challenges for the actuators. The extended SMC methods have been developed to suppress the chattering. The boundary layer based SMC method is commonly used by introducing boundary layer into control system to replace the sign function [25]. The thickness of the boundary layer contributes to trade-off relationships between the control accuracy and chattering suppression, and it demonstrates a limited effect in chattering reduction of SMC method for the nonlinear under-actuated systems. The other extended SMC approaches, such as high order SMC [26] and terminal SMC [27], [28] were extensively applied in the quadrotor UAV system to overcome the deficiency of chattering phenomenon in SMC. It is noted that the design of the nonlinear sliding surface in the high order or terminal SMC is cumbersome, and the calculation of the coefficients is complicated. Recently, the model-free intelligent control approaches including the fuzzy control system and the neural networks have been increasingly used for the multi-rotor UAV to counteract the disturbances and accommodate the control efforts to the parameter changes [29]–[33]. However, the complex fuzzy rules and tedious learning process existing in the intelligent control system always require larger computational efforts.

Backstepping control is an acclaimed nonlinear control strategy and has received great attention from many researchers [34]–[36]. Owing to the systematic and recursive design methodology based on Lyapunov theorem, the backstepping control scheme is well suited for the coupled and under-actuated system with nonlinearities, especially for the multi-rotor UAV [37]. In [38], the backstepping strategy was applied for the payload dropping control of a quadrotor helicopter, and the roll angle fluctuated at the moment of payload dropping. In [39], the backstepping controller was used to force the hexacopter UAV system to follow a reference trajectory. Despite the popularity and advantage of the backstepping method, it is sensitive to the disturbances, and control performances will be degraded when the parameter uncertainties and external perturbations occur. To overcome the drawback of the sensitivity to the uncertainties, further efforts have been made on the enhanced backstepping approaches [40]–[45], among which the observers based one has been extensively used. The robustness of the observers based control stems from the satisfactory performances of the observer in estimating and compensating uncertainties and disturbances [46], [47]. Various forms of disturbance observers have been applied in the back-stepping and other control schemes. In [48], a sliding mode observer based backstepping control was proposed for the hexacopter to estimate and compensate for the effect of wind parameters. In [49], an adaptive back-stepping sliding mode control was developed for the attitude control of a humanoid robot dual manipulator, and excessive chattering was avoided by introducing a nonlinear disturbance observer (NDO) to compensate for uncertainties. In [50], [51], neural networks(NN)-based observers were applied in the backstepping approach to approximate the uncertainties existing in the system dynamics. Among the disturbance observers, the nonlinear extended stated observer originally proposed by Han [52] is an active way to estimate not only the external disturbance but also the plant dynamics, through which the requirement on the accurate model can be relaxed. To make the ESO more practical to implement, Gao [53] modified it into a linear version [54]. In [55], a linear ESO was developed to estimate total uncertainty, and the robust LESO based output-feedback control was built for the path-following of the autonomous underwater vehicles. Noting that, (1) most of the disturbance observers mentioned above were thoroughly developed on the position feedback, which is commonly obtained by integrating the velocity information of the system, especially for the multi-rotor UAVs. The long-time integration errors will influence the position information, which further degrades estimation accuracy of the observers. (2) Besides, the observers were thoroughly developed based on assumptions that the disturbances or the derivative of one are bounded, and the observation errors are closely related to the bounds of the disturbances or the derivatives. Indeed, the relative large observation errors will be induced when the disturbance changes, which will degrade the robust flight performances of the multi-rotor UAV. To decrease the observation errors, large control gains are generally selected, but the measurement noise will be magnified and peaking phenomena will be induced. The high gain behaviors will degrade the control performance and even deteriorate the system stability. It is worth mentioning that the adaptive scheme is an efficient method for motion control [56]–[58], and it exhibits superior performances in handling bounded uncertainties.

Motivated by the aforementioned works, this paper proposes a nonlinear robust and adaptive backstepping control scheme for the hexacopter system. The nonlinear control scheme is hierarchically developed. The nominal backstepping control is fully designed as the main controller to achieve a fundamental flight performance. Next, the robust compensator based on the $2^{nd}$-order linear extended state observer with velocity feedback (LESO-VF) is employed in the backstepping control scheme to estimate and compensate the uncertainties and external disturbances, through which the effect of instabilities is suppressed and robust flight capability is guaranteed. Also, to avoid high gain behaviors of the LESO, an adaptive switching term based compensator is introduced to counteract observation errors, and the enhanced robustness is achieved.

The main contributions can be summarized as follows:

(1) Compared with the neural networks (NN)-based observers [30]–[33], [50], [51] and the nonlinear ESO [59]–[62] requiring the multiple states information and complex nonlinear coefficients, the LESO employed in the control scheme is intuitively designed based on the state feedback, and the tuning operation is rather simple since linear observer parameters are utilized.

(2) Rather than the nonlinear disturbances observers [45]–[49], [64]–[67] and other ESO [59]–[63] based on the position feedback, the $2^{nd}$-order LESO with velocity feedback is developed. In practice, the velocity information is easily acquired, which is more accurate and reliable, especially for the multi-rotor UAVs. Besides, the initial velocities of the hexacopter UAV are zero, which are equal to the initial state values of observers set to be zero without loss of generality. The peaking phenomenon caused by the initial errors can be avoided. Therefore, the $2^{nd}$-order LESO based on the velocity feedback is likely to be more practical than that with the position feedback.

(3) Unlike the existing observers [59]–[67] including ESO based control methods with large observer gains being usually selected to reduce the bounded tracking errors, the proposed nonlinear control scheme improves the robustness by introducing the adaptive switching term based compensator to eliminate the observation errors, and the asymptotical tracking performance of the hexacopter UAV can be achieved. The requirement on the large observer gains is relaxed, and high gain behaviors can be avoided.

The remainder of this paper is organized as follows: Nonlinear model of the hexacopter UAV and the control problems are formulated in Section II. In Section III, the robust and adaptive backstepping control scheme is hierarchically developed, and the Lyapunov analysis ensures the tracking errors of the hexacopter system asymptotically converge to zero. Comparative trajectory tracking of the hexacopter UAV is conducted in the simulation environment in Section IV to verify the efficiency and superiority of the proposed control scheme. Finally, conclusions are presented in Section V.

## II. HEXACOPTER MODEL AND PROBLEM STATEMENT

The hexacopter UAV is a nonlinear, coupled and underactuated system with 6-DOF but only four actual inputs. It has a rigid symmetrical configuration consisted of six rotors symmetrically mounted on the airframe, as is shown in Fig. 1. The motions of the hexacopter UAV are fulfilled by regulating the six rotors, among which Rotors (1, 3, 5) rotate in the counter-clockwise (CCW), while Rotors (2, 4, 6) rotate in the opposite direction to adjust the yaw angle-$\{\psi\}$. Differentiating the speed of Rotors (1, 2) and Rotors (4, 5) generates the pitch-$\{\theta\}$ rotation, which contributes the movement in $x$- axis direction. Besides, the differential speed of Rotors (1, 5, 6) and Rotors (2, 3, 4) propels the roll-$\{\phi\}$ motion, corresponding to the lateral movement along the $y$-axis.

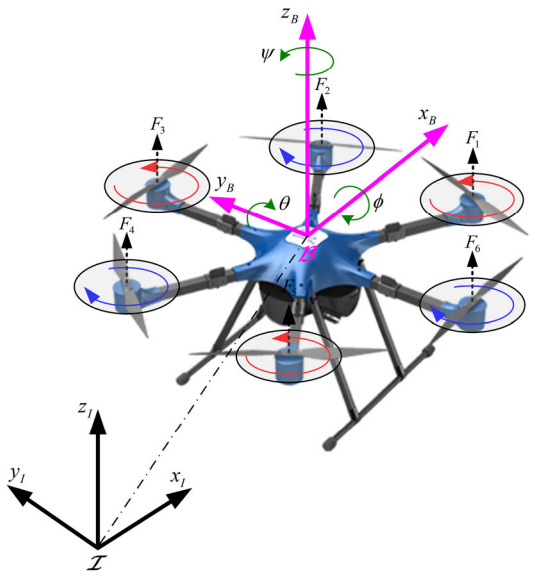


**FIGURE 1.** Schematic diagram of the hexacopter UAV.

Furthermore, the vertical movement along the $z$-axis is realized by changing the speed of all the rotors collectively.

The hexacopter dynamic model is established via the Newton-Euler formulism. Two coordinate systems, including the inertial reference frame ($\mathcal{I}$ - frame) and the body-fixed one ($\mathcal{B}$ - frame) are built respectively, as is depicted in Fig. 1. The hexacopter dynamics can be described as

$$\begin{cases} \prod\limits_{\text{Translation}} (\boldsymbol{P}) & \begin{cases} \dot{\boldsymbol{P}} = \boldsymbol{v} \\ m\dot{\boldsymbol{v}} = -mg\boldsymbol{e}_z + \boldsymbol{T}_{\mathcal{B}}^{\mathcal{I}}(\boldsymbol{\Theta})\boldsymbol{F}_f + \boldsymbol{F}_d \end{cases} \\ \prod\limits_{\text{Rotation}} (\boldsymbol{\Theta}) & \begin{cases} \dot{\boldsymbol{\Theta}} = \boldsymbol{R}_{\mathcal{B}}^{\mathcal{I}}(\boldsymbol{\Theta})\boldsymbol{\omega} \\ \boldsymbol{J}\dot{\boldsymbol{\omega}} = -\boldsymbol{\omega} \times \boldsymbol{J}\boldsymbol{\omega} + \boldsymbol{\Gamma}_f + \boldsymbol{\Gamma}_g + \boldsymbol{\Gamma}_d \end{cases} \end{cases} \tag{1}$$

where $\boldsymbol{P} = [x, y, z]^T$ is the Euclidean position in $\mathcal{I}$ - frame; $\boldsymbol{\Theta} = [\phi, \theta, \psi]^T$ denotes the three Euler angles; $\boldsymbol{e}_z = [0, 0, 1]^T$ represents a vector along the $z$-axis; $(-\omega \times J\omega)$ yields the gyroscopic effect, with $\boldsymbol{\omega} \in \Re^3$ being the angular velocity, and $\boldsymbol{J} = diag\left[I_x, I_y, I_z\right] \in \Re^{3\times3}$ is the inertia matrix.

$\boldsymbol{T}_{\mathcal{B}}^{\mathcal{I}}(\Theta)$ and $\boldsymbol{R}_{\mathcal{B}}^{\mathcal{I}}(\Theta)$ are the translation matrices from the $\mathcal{B}$ - frame to the $\mathcal{I}$ - frame, expressed as

$$\begin{cases} \boldsymbol{T}_{\mathcal{B}}^{\mathcal{I}}(\Theta) = \begin{bmatrix} c_\theta c_\psi & s_\phi s_\theta c_\psi - c_\phi s_\psi & c_\phi s_\theta c_\psi + s_\phi s_\psi \\ c_\theta s_\psi & s_\phi s_\theta s_\psi + c_\phi c_\psi & c_\phi s_\theta s_\psi - s_\phi c_\psi \\ -s_\theta & s_\phi c_\theta & c_\phi c_\theta \end{bmatrix} \\ \boldsymbol{R}_{\mathcal{B}}^{\mathcal{I}}(\Theta) = \begin{bmatrix} 1 & s_\phi t_\theta & c_\phi t_\theta \\ 0 & c_\phi & -s_\phi \\ 0 & s_\phi / c_\theta & c_\phi / c_\theta \end{bmatrix} \end{cases} \tag{2}$$

where $s_{(\cdot)} = sin(\cdot)$, $c_{(\cdot)} = cos(\cdot)$, $t_{(\cdot)} = tan(\cdot)$. In the cases where hexacopter performs rotations of low amplitude, $\boldsymbol{R}_{\mathcal{B}}^{\mathcal{I}}(\Theta)$ is very close to an identity matrix.

$\boldsymbol{F}_f = [0, 0, u_1]^T$ and $\boldsymbol{\Gamma}_f = [u_2, u_3, u_4]^T$ are the control forces and torques in $\mathcal{B}$ - frame, where $u_{1-4}$ can be developed

as

$$\begin{cases} u_1 = F_1 + F_2 + F_3 + F_4 + F_5 + F_6 \\ u_2 = -\frac{1}{2}F_1 l + \frac{1}{2}F_2 l + F_3 l + \frac{1}{2}F_4 l - \frac{1}{2}F_5 l - F_6 l_6 \\ u_3 = -\frac{\sqrt{3}}{2}F_1 l - \frac{\sqrt{3}}{2}F_2 l + \frac{\sqrt{3}}{2}F_4 l + \frac{\sqrt{3}}{2}F_5 l \\ u_4 = C_d\left(-\Omega_1^2 + \Omega_2^2 - \Omega_3^2 + \Omega_4^2 - \Omega_5^2 + \Omega_6^2\right) \end{cases} \tag{3}$$

where the force $F_i$ generated by $i$-th rotor is approximated as $F_i = K_p\Omega_i^2$, $K_p \in \Re^+$ denotes the thrust coefficient of the propeller, $C_d \in \Re^+$ is the drag coefficient, and $\Omega_i$ represents the speed of Rotor- $i$.

$\mathbf{\Gamma}_g$ represents the gyroscopic impact owing to the propeller orientation change expressed as

$$\mathbf{\Gamma}_g = \sum_{i=1}^{6} J_r\left(\boldsymbol{\omega} \times \boldsymbol{e}_z\right)\bar{\Omega} \tag{4}$$

where $J_r \in \Re^+$ denotes the rotational inertia of the propeller, $\bar{\Omega} = \Omega_1 - \Omega_2 + \Omega_3 - \Omega_4 + \Omega_5 - \Omega_6$.

$\boldsymbol{F}_d$ and $\mathbf{\Gamma}_d$ are the whole disturbances $\boldsymbol{w}_d$ including parameter uncertainties and external disturbances, such as parameter changes, asymmetric structures, payload variation, rotor fluctuation, and aerodynamic drags, etc, denoted as

$$\begin{cases} \boldsymbol{F}_d = \boldsymbol{w}_P = \left[w_x, w_y, w_z\right]^T \\ \mathbf{\Gamma}_d = \boldsymbol{w}_\Theta = \left[w_\phi, w_\theta, w_\psi\right]^T \end{cases} \tag{5}$$

Consequently, combining Eqs. (1-5) yields the dynamic model of the hexacopter UAV as

$$\begin{cases} \prod\limits_{\text{Translation}} (\boldsymbol{P}) & \begin{cases} \ddot{x} = \left(c_\phi s_\theta c_\psi + s_\phi s_\psi\right)\frac{1}{m}u_1 + w_x \\ \ddot{y} = \left(c_\phi s_\theta s_\psi - s_\phi c_\psi\right)\frac{1}{m}u_1 + w_y \\ \ddot{z} = -g + \left(c_\phi c_\theta\right)\frac{1}{m}u_1 + w_z \end{cases} \\ \prod\limits_{\text{Rotation}} (\boldsymbol{\Theta}) & \begin{cases} \ddot{\phi} = \dot{\theta}\dot{\psi}\left(\frac{I_y - I_z}{I_x}\right) - \frac{J_r}{I_x}\dot{\theta}\bar{\Omega} + \frac{l}{I_x}u_2 + w_\phi \\ \ddot{\theta} = \dot{\phi}\dot{\psi}\left(\frac{I_z - I_x}{I_y}\right) + \frac{J_r}{I_y}\dot{\phi}\bar{\Omega} + \frac{l}{I_y}u_3 + w_\theta \\ \ddot{\psi} = \dot{\theta}\dot{\phi}\left(\frac{I_x - I_y}{I_z}\right) + \frac{1}{I_z}u_4 + w_\psi \end{cases} \end{cases} \tag{6}$$

To facilitate control design, the dynamic model of the hexacopter system considering the whole disturbances can be represented in the nonlinear state equation as follows

$$\ddot{\boldsymbol{X}} = \boldsymbol{G}\boldsymbol{u} + \boldsymbol{f}\left(X\right) + \boldsymbol{w}_d \tag{7}$$

where $\boldsymbol{u}$, $\boldsymbol{X}$ and $\boldsymbol{w}_d$ are the control inputs, states, and whole disturbances vector developed as follows

$$\boldsymbol{u} = \left[u_x, u_y, u_z, u_2, u_3, u_4\right]^T \in \Re^6 \tag{8}$$

$$\boldsymbol{X} = \left[x_1, x_2, x_3, x_4, x_5, x_6\right]^T = \left[x, y, z, \phi, \theta, \psi\right]^T \in \Re^6 \tag{9}$$

$$\boldsymbol{w}_d = \left[w_1, w_2, \ldots, w_6\right]^T = \left[w_x, w_y, w_z, w_\phi, w_\theta, w_\psi\right]^T \in \Re^6 \tag{10}$$

and the functions $\boldsymbol{f}(X)$ and $\boldsymbol{G}$ are described accordingly as

$$\boldsymbol{f}\left(X\right) = \begin{pmatrix} 0 \\ 0 \\ 0 \\ \dot{\theta}\dot{\psi}a_1 - a_2\dot{\theta}\bar{\Omega} \\ \dot{\phi}\dot{\psi}a_3 + a_4\dot{\phi}\bar{\Omega} \\ \dot{\theta}\dot{\phi}a_5 \end{pmatrix}, \quad \boldsymbol{G} = \begin{pmatrix} 1 & 0 & 0 & 0 & 0 & 0 \\ 0 & 1 & 0 & 0 & 0 & 0 \\ 0 & 0 & 1 & 0 & 0 & 0 \\ 0 & 0 & 0 & b_1 & 0 & 0 \\ 0 & 0 & 0 & 0 & b_2 & 0 \\ 0 & 0 & 0 & 0 & 0 & b_3 \end{pmatrix} \tag{11}$$

respectively, among which $a_1 = (I_y - I_z)/I_x$, $a_2 = J_r/I_x$, $a_3 = (I_z - I_x)/I_y$, $a_4 = J_r/I_y$, $a_5 = (I_x - I_y)/I_z$, $b_1 = l/I_x$, $b_2 = l/I_y$, $b_3 = 1/I_z$.

The control objective is to ensure the hexacopter UAV a robust trajectory tracking performance against the parameter uncertainties and external disturbances. Due to the under-actuated property of the hexacopter system, it is impossible to regulate the 6-DOF outputs by only four control inputs $u_{1-4}$. Considering the coupled relationship between the translational and rotational dynamics, the positional translation can be controlled indirectly by rotations, and two auxiliary control inputs are selected as $\{\phi_d, \theta_d\}$. More specifically, the total lift forces together with the attitudes yield the component forces along the $\{x, y, z\}$ axis, which contributes the positional movements of the hexacopter UAV. To fulfill the specified trajectory tracking, the corresponding attitudes of the hexacopter UAV are needed. To solve the desired attitudes, the following equations are deduced from (6) as

$$\begin{cases} u_x = \left(\cos\phi_d \sin\theta_d \cos\psi_d + \sin\phi_d \sin\psi_d\right)\frac{1}{m}u_1 \\ u_y = \left(\cos\phi_d \sin\theta_d \sin\psi_d - \sin\phi_d \cos\psi_d\right)\frac{1}{m}u_1 \\ u_z = -g + \left(\cos\phi_d \cos\theta_d\right)\frac{1}{m}u_1 \end{cases} \tag{12}$$

where the control inputs $u_{x,y,z}$ for the movements along $\{x, y, z\}$ can be fully acquired in (41) in Section III, and the designated $\psi_d$ is prior known, which implies that there exist three unknown terms $\{u_1, \phi_d, \theta_d\}$ to be calculated in (12). The transfer function from $u_{x,y,z}$ to $\{u_1, \phi_d, \theta_d\}$ can be solved as

$$\begin{cases} u_1 = m\sqrt{u_x^2 + u_y^2 + (u_z + g)^2} \\ \phi_d = \arcsin\left(\dfrac{u_x \sin\psi - u_y \cos\psi}{\sqrt{u_x^2 + u_y^2 + (u_z + g)^2}}\right) \\ \theta_d = \arctan\left(\dfrac{u_x \cos\psi + u_y \sin\psi}{u_z + g}\right) \end{cases} \tag{13}$$

## III. ROBUST AND ADAPTIVE CONTROL DESIGN

In this section, the derivation of the proposed control scheme for the hexacopter UAV is progressively developed as follows: (1) The nominal backstepping strategy is initially designed as the main controller for the fundamental flight trajectory tracking. (2) To ensure the hexacopter UAV a robust flight capability, the LESO based robust compensator with different states (position and velocity) feedback is introduced to observe and compensate for the parameter uncertainties

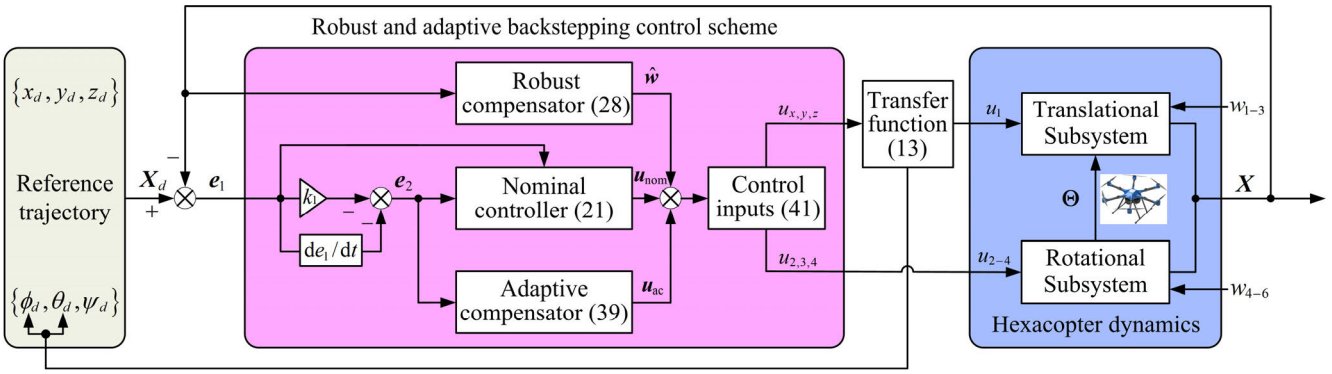


**FIGURE 2.** Control architecture of the proposed control scheme for the hexacopter UAV.

and external disturbances. (3) To further improve the robustness, a switching term based adaptive compensator is cooperatively employed to compensate for the observation errors generated by the LESO. Considering the under-actuated and coupled properties, the hexacopter dynamics is decomposed into the translational and rotational subsystems, the relationship between which is established through (13). The overall control scheme is illustrated in Fig. 2, and detailed descriptions of each control effort are hierarchically exhibited in following subsections.

### A. NOMINAL BACKSTEPPING CONTROL SYSTEM

The backstepping control is an acclaimed nonlinear control strategy, and its advantage lies in design flexibility because of the recursive utilization of Lyapunov functions. The stability of the total control system can be guaranteed by the final actual control law generated by the systematic and recursive design methodology.

In this subsection, the nominal backstepping control is designed as the main controller for the hexacopter system to achieve the fundamental flight tracking performance. The design of the nominal main controller is presented as follows:

**Step I:** Define the tracking error $\boldsymbol{e}_1 = \{e_{11}, e_{12}, \ldots, e_{16}\}^T \in \Re^6$ as follows

$$\boldsymbol{e}_1 = \boldsymbol{X}_d - \boldsymbol{X} \tag{14}$$

Taking the derivative of (14) yields

$$\dot{\boldsymbol{e}}_1 = \dot{\boldsymbol{X}}_d - \dot{\boldsymbol{X}} \tag{15}$$

Then, we take a virtual control input $\dot{\boldsymbol{X}}_v \in \Re^6$ for $\dot{\boldsymbol{X}}$ as

$$\dot{\boldsymbol{X}}_v = \dot{\boldsymbol{X}}_d + \boldsymbol{k}_1 \boldsymbol{e}_1 \tag{16}$$

where $\boldsymbol{k}_1 = diag(k_{11}, k_{12}, \ldots, k_{16}) \in \Re^+_{6\times6}$ is a positive diagonal control gain matrix.

**Step II:** Define the deviation of the virtual control from its desired value as

$$\boldsymbol{e}_2 = \dot{\boldsymbol{X}} - \dot{\boldsymbol{X}}_v = \dot{\boldsymbol{X}} - \dot{\boldsymbol{X}}_d - \boldsymbol{k}_1 \boldsymbol{e}_1 \tag{17}$$

Differentiating (17) yields

$$\dot{\boldsymbol{e}}_2 = \ddot{\boldsymbol{X}} - \ddot{\boldsymbol{X}}_v = \boldsymbol{G}\boldsymbol{u} + \boldsymbol{f}(X) + \boldsymbol{w}_d - \ddot{\boldsymbol{X}}_d - \boldsymbol{k}_1 \dot{\boldsymbol{e}}_1 \tag{18}$$

Choose the Lyapunov function as

$$V(\boldsymbol{e}_1, \boldsymbol{e}_2) = \frac{1}{2}\boldsymbol{e}_1^T \boldsymbol{e}_1 + \frac{1}{2}\boldsymbol{e}_2^T \boldsymbol{e}_2 \tag{19}$$

Taking the derivative of (19) yields

$$\begin{aligned} &\dot{V}(\boldsymbol{e}_1, \boldsymbol{e}_2) \\ &= \boldsymbol{e}_1^T \dot{\boldsymbol{e}}_1 + \boldsymbol{e}_2^T \dot{\boldsymbol{e}}_2 \\ &= \boldsymbol{e}_1^T \left(\dot{\boldsymbol{X}}_d - \dot{\boldsymbol{X}}\right) + \boldsymbol{e}_2^T \left(\boldsymbol{G}\boldsymbol{u} + \boldsymbol{f}(X) + \boldsymbol{w}_d - \ddot{\boldsymbol{X}}_d - \boldsymbol{k}_1 \dot{\boldsymbol{e}}_1\right) \\ &= \boldsymbol{e}_1^T \left(-\boldsymbol{e}_2 - \boldsymbol{k}_1 \boldsymbol{e}_1\right) + \boldsymbol{e}_2^T \left(\boldsymbol{G}\boldsymbol{u} + \boldsymbol{f}(X) + \boldsymbol{w}_d - c\ddot{\boldsymbol{X}}_d - \boldsymbol{k}_1 \dot{\boldsymbol{e}}_1\right) \end{aligned} \tag{20}$$

**Step III:** Assuming the whole disturbances in (7) are well known, the practical nominal control input can be achieved as

$$\boldsymbol{u} := \boldsymbol{u}_{nom} = \boldsymbol{G}^{-1}\left(\ddot{\boldsymbol{X}}_d + \boldsymbol{k}_1 \dot{\boldsymbol{e}}_1 - \boldsymbol{f}(X) - \boldsymbol{w}_d + \boldsymbol{e}_1 - \boldsymbol{k}_2 \boldsymbol{e}_2\right) \tag{21}$$

where $\boldsymbol{k}_2 = diag(k_{21}, k_{22}, \ldots, k_{26}) \in \Re^+_{6\times6}$ is a positive diagonal control gain matrix.

Substituting (21) into (20) yields

$$\begin{aligned} \dot{V}(\boldsymbol{e}_1, \boldsymbol{e}_2) &= -\boldsymbol{e}_1^T \boldsymbol{k}_1 \boldsymbol{e}_1 - \boldsymbol{e}_2^T \boldsymbol{k}_2 \boldsymbol{e}_2 \\ &= \sum_{i=1}^{6} -k_{1i}\boldsymbol{e}_{1i}^2 - k_{2i}\boldsymbol{e}_{2i}^2 \le 0 \end{aligned} \tag{22}$$

### B. ROBUST LINEAR EXTENDED STATE OBSERVER (LESO) COMPENSATOR

The analysis above is developed assuming that the hexacopter UAV is a nominal model, i.e., disturbances existing in the hexacopter dynamics are prior known. Indeed, parameter uncertainties and external disturbances perturbing the hexacopter system are unknown factors, which may result in performance degradation and unexpected instabilities. Here, the $3^{rd}$-order LESO based on position feedback and the $2^{nd}$-order LESO based on velocity feedback are contrastively introduced as robust compensators to suppress the effects of the parameter uncertainties and external disturbances on the hexacopter system.

#### 1) $3^{RD}$-ORDER LESO BASED ON POSITION FEEDBACK

To facilitate the observer design, the $3^{rd}$-order extended state dynamic model from (7) can be achieved as

$$\dot{\mathbf{x}} = \boldsymbol{A}\mathbf{x} + \boldsymbol{B}_1[\boldsymbol{G}\boldsymbol{u} + \boldsymbol{f}(X)] + \boldsymbol{B}_2\dot{\boldsymbol{w}}_d \tag{23}$$

where, $\mathbf{x} = \begin{bmatrix} \boldsymbol{X} \\ \dot{\boldsymbol{X}} \\ \boldsymbol{w}_d \end{bmatrix} \in \Re^{18}$, $\boldsymbol{A} = \begin{bmatrix} \boldsymbol{O}_{6\times6} & \boldsymbol{I}_{6\times6} & \boldsymbol{O}_{6\times6} \\ \boldsymbol{O}_{6\times6} & \boldsymbol{O}_{6\times6} & \boldsymbol{I}_{6\times6} \\ \boldsymbol{O}_{6\times6} & \boldsymbol{O}_{6\times6} & \boldsymbol{O}_{6\times6} \end{bmatrix} \in \Re^{18\times18}$, $\boldsymbol{B}_1 = \begin{bmatrix} \boldsymbol{O}_{6\times6} \\ \boldsymbol{I}_{6\times6} \\ \boldsymbol{O}_{6\times6} \end{bmatrix} \in \Re^{18\times6}$, $\boldsymbol{B}_2 = \begin{bmatrix} \boldsymbol{O}_{6\times6} \\ \boldsymbol{O}_{6\times6} \\ \boldsymbol{I}_{6\times6} \end{bmatrix} \in \Re^{18\times6}$, and $\dot{\boldsymbol{w}}_d \in \Re^6$ denotes the derivative of the whole disturbances $\boldsymbol{w}_d$.

By the system (23), the $3^{rd}$-order LESO for the hexacopter UAV is designed as

$$\dot{\hat{\mathbf{x}}} = \boldsymbol{A}\hat{\mathbf{x}} + \boldsymbol{B}_1[\boldsymbol{G}\boldsymbol{u} + \boldsymbol{f}(X)] + \boldsymbol{K}\left(\mathbf{x} - \hat{\mathbf{x}}\right) \tag{24}$$

where $\hat{\mathbf{x}} = [\hat{\boldsymbol{X}}, \hat{\dot{\boldsymbol{X}}}, \hat{\boldsymbol{w}}_d]^T$ are observations of the extended states $\mathbf{x}$, $\boldsymbol{K} = \begin{bmatrix} \boldsymbol{k}_{O1}/\varepsilon & \boldsymbol{O}_{6\times6} & \boldsymbol{O}_{6\times6} \\ \boldsymbol{k}_{O2}/\varepsilon^2 & \boldsymbol{O}_{6\times6} & \boldsymbol{O}_{6\times6} \\ \boldsymbol{k}_{O3}/\varepsilon^3 & \boldsymbol{O}_{6\times6} & \boldsymbol{O}_{6\times6} \end{bmatrix} \in \Re^{18\times18}$ is the control gain matrix, where $\boldsymbol{k}_{O1} = diag(k_{11}, k_{12}, \ldots, k_{16})$, $\boldsymbol{k}_{O2} = diag(k_{21}, k_{22}, \ldots, k_{26})$, $\boldsymbol{k}_{O3} = diag(k_{31}, k_{32}, \ldots, k_{36})$,with $\boldsymbol{k}_{O1-3} \in \Re^{+}_{6\times6}$ and $\varepsilon \in \Re^{+}$ being designed for staying positive definite diagonal matrix.

*Remark 1:* The control gain matrix $\boldsymbol{K}$ implies that the position information is needed in the feedback control loop.

Subtracting (24) from (23) yields

$$\dot{\mathbf{e}} = \bar{\boldsymbol{A}}\mathbf{e} + \boldsymbol{B}_2\dot{\boldsymbol{w}}_d \tag{25}$$

where the observation errors of the disturbance observer are $\mathbf{e} = [\tilde{\boldsymbol{X}}, \tilde{\dot{\boldsymbol{X}}}, \tilde{\boldsymbol{w}}_d]^T = [\boldsymbol{X} - \hat{\boldsymbol{X}}, \dot{\boldsymbol{X}} - \hat{\dot{\boldsymbol{X}}}, \boldsymbol{w}_d - \hat{\boldsymbol{w}}_d]^T \in \Re^{18}$, $\bar{\boldsymbol{A}} = \boldsymbol{A} - \boldsymbol{K}$. The candidate control gains $\boldsymbol{k}_{O1}$, $\boldsymbol{k}_{O2}$ and $\boldsymbol{k}_{O3}$ are chosen appropriately to let $\bar{\boldsymbol{A}}$ satisfy the Hurwitz stability criterions, i.e., $\left|\lambda \boldsymbol{I}_{18} - \bar{\boldsymbol{A}}\right| = \prod_{i=1}^{18}(\lambda + \lambda_i) = 0$. $\lambda_i$ is the matrix eigenvalue of $\bar{\boldsymbol{A}}$ and meets $0 < \lambda_i \leq \lambda_j\ (i < j, i, j = 1, 2, \ldots, 18)$.

Then, the solution of (25) can be achieved as

$$\mathbf{e}(t) = \exp\left(\bar{\boldsymbol{A}}t\right)\mathbf{e}(0) + \int_0^t \exp\left(\bar{\boldsymbol{A}}(t-\ell)\right)\boldsymbol{B}_2\dot{\boldsymbol{w}}_d d\ell \tag{26}$$

Assuming that the derivative of disturbances is constrained in a reasonable domain such that $\sup_{t\in[0,\infty]} \|\dot{\boldsymbol{w}}_d\| \leq M_w$, we can obtain the solution of (25) as

$$\begin{aligned} \|\mathbf{e}(t)\| &\leq \left\|\exp\left(\bar{\boldsymbol{A}}t\right)\mathbf{e}(0)\right\| + \left\|\int_0^t \exp\left(\bar{\boldsymbol{A}}(t-\ell)\right)\boldsymbol{B}_2\dot{\boldsymbol{w}}_d d\ell\right\| \\ &\leq \beta\|\mathbf{e}(0)\|\exp(-\lambda_1 t) + \frac{\beta M_w}{\lambda_1}(1 - \exp(-\lambda_1 t)) \\ &\leq \beta\|\mathbf{e}(0)\| + \frac{\beta M_w}{\lambda_1} = M_e \end{aligned} \tag{27}$$

where $\beta \in \Re^{+}$. According to the analysis above, it can be obtained that the observation errors of the $3^{rd}$-order LESO is bounded in a compact set, i.e., $\left\|\tilde{\boldsymbol{X}}\right\|, \left\|\tilde{\dot{\boldsymbol{X}}}\right\|, \|\tilde{\boldsymbol{w}}_d\| \leq M_e$.

*Remark 2:* The control gain matrix $\boldsymbol{K}$ in (24) governs the approximation rate of observations $\hat{\mathbf{x}}$ to the real extended states $\mathbf{x}$. The larger $k_{pr}(p = 1, 2, 3; r = 1, 2, \ldots, 6)$ and smaller in $\boldsymbol{K}$ contributes to a faster and higher-precision convergence. However, the overlarge control gains will magnify the measurement noise in the estimated states and induce the peaking phenomena, and then the system is likely to be unstable [68]. Therefore, the effects of the parameter uncertainties and external disturbances on the system cannot be sufficiently suppressed in practice only by the LESO compensation.

#### 2) $2^{ND}$-ORDER LESO BASED ON VELOCITY FEEDBACK

Similar to the $3^{rd}$-order LESO (24), the decreased $2^{nd}$-order LESO for the hexacopter UAV is designed as

$$\dot{\hat{\boldsymbol{\chi}}} = \boldsymbol{A}'\hat{\boldsymbol{\chi}} + \boldsymbol{B}_1'[\boldsymbol{G}\boldsymbol{u} + \boldsymbol{f}(X)] + \boldsymbol{L}\left(\boldsymbol{\chi} - \hat{\boldsymbol{\chi}}\right) \tag{28}$$

where $\hat{\boldsymbol{\chi}} = [\hat{\dot{\boldsymbol{X}}}, \hat{\boldsymbol{w}}_d]^T \in \Re^{12}$ are observations of the dynamic states $\boldsymbol{\chi} = [\dot{\boldsymbol{X}}, \boldsymbol{w}_d]^T$, $\boldsymbol{A}' = \begin{bmatrix} \boldsymbol{O}_{6\times6} & \boldsymbol{I}_{6\times6} \\ \boldsymbol{O}_{6\times6} & \boldsymbol{O}_{6\times6} \end{bmatrix} \in \Re^{12\times12}$, $\boldsymbol{B}_1' = \begin{bmatrix} \boldsymbol{I}_{6\times6} \\ \boldsymbol{O}_{6\times6} \end{bmatrix} \in \Re^{12\times6}$, $\boldsymbol{L} = \begin{bmatrix} \boldsymbol{l}_{O1}/\rho & \boldsymbol{O}_{6\times6} \\ \boldsymbol{l}_{O2}/\rho^2 & \boldsymbol{O}_{6\times6} \end{bmatrix}$ is the control gain matrix of the observer, where $\boldsymbol{l}_{O1} = diag\,(l_{11}, l_{12}, \ldots, l_{16})$, $\boldsymbol{l}_{O2} = diag\,(l_{21}, l_{22}, \ldots, l_{26})$ with $\boldsymbol{l}_{O1-2} \in \Re^{+}_{6\times6}$ and $\rho \in \Re^{+}$ being designed for staying positive definite diagonal matrix.

*Remark 3:* The control gain matrix $\boldsymbol{L}$ implies that only the velocity is needed in the feedback control loop. Therefore, the integral errors of the velocity for time can be avoided. Generally, the UAV starts taking-off in 0-velocity equal to the initial states of the LESO, and the initial errors fed back into the LESO are 0. Therefore, the peaking phenomenon can be avoided.

Similar to the stability analysis of the $3^{rd}$-order LESO, we can obtain the observation errors of the $2^{nd}$-order LESO as

$$\dot{\tilde{\boldsymbol{\chi}}} = \bar{\boldsymbol{A}}'\tilde{\boldsymbol{\chi}} + B_2'\dot{\boldsymbol{w}}_d \tag{29}$$

where $\tilde{\boldsymbol{\chi}} = [\tilde{\dot{\boldsymbol{X}}}, \tilde{\boldsymbol{w}}_d]^T = [\dot{\boldsymbol{X}} - \hat{\dot{\boldsymbol{X}}}, \boldsymbol{w}_d - \hat{\boldsymbol{w}}_d]^T \in \Re^{12}$, $\bar{\boldsymbol{A}}' = \boldsymbol{A}' - \boldsymbol{L}$, $\boldsymbol{B}_2' = \begin{bmatrix} \boldsymbol{O}_{6\times6} \\ \boldsymbol{I}_{6\times6} \end{bmatrix} \in \Re^{12\times6}$. The observation error $\tilde{\boldsymbol{\chi}}$ is converged into a compact set $\|\tilde{\boldsymbol{\chi}}(t)\| \leq M_{\boldsymbol{\chi}}$, i.e., $\left\|\tilde{\dot{\boldsymbol{X}}}\right\|$, $\|\tilde{\boldsymbol{w}}_d\| \leq M_{\boldsymbol{\chi}}$. The larger $l_{qr}\ (q = 1, 2; r = 1, 2, \ldots, 6)$ and smaller $\rho$ in $\boldsymbol{L}$ contribute to a higher-precision convergence.

Therefore, combining with (21) and (28), the linear extended state observer based backstepping controller can be obtained as

$$\boldsymbol{u} = \boldsymbol{G}^{-1}\left(\ddot{\boldsymbol{X}}_d + \boldsymbol{k}_1\dot{\boldsymbol{e}}_1 - \boldsymbol{f}(X) - \hat{\boldsymbol{w}}_d + \boldsymbol{e}_1 - \boldsymbol{k}_2\boldsymbol{e}_2\right) \tag{30}$$

#### 3) STABILITY OF THE ROBUST CONTROL SYSTEM

*Lemma 1* (Petros and Jing [69]): In view of $V : [0, \infty) \in \Re$, the solution of the inequality $\dot{V} \leq -\alpha V + f, \forall t \geq t_0 \geq 0$ is as follows:

$$V(t) \leq e^{-\alpha(t-t_0)}V(t_0) + \int_{t_0}^t e^{-\alpha(t-\ell)}f(\ell)\,\mathrm{d}\ell \tag{31}$$

where, $\alpha$ is an arbitrary constant.

*Theorem 1:* Consider the dynamic system (7) perturbed by the parameter uncertainties and external disturbances, the proposed robust backstepping control scheme (30) with the compensation of the disturbances can ensure that the system outputs of the hexacopter UAV converge to the designated flight trajectory, i.e., $\boldsymbol{e}_1$ and $\boldsymbol{e}_2$ are bounded in a compact set.

*Proof:* Choose the following Lyapunov function

$$V_1 = \frac{1}{2}\boldsymbol{e}_1^T\boldsymbol{e}_1 + \frac{1}{2}\boldsymbol{e}_2^T\boldsymbol{e}_2 = \frac{1}{2}\sum_{i=1}^{6}\left(e_{1i}^2 + e_{2i}^2\right) \tag{32}$$

Taking the derivative of (32) and combining (18,30) yields

$$\begin{aligned}\dot{V}_1 &= \boldsymbol{e}_1^T\dot{\boldsymbol{e}}_1 + \boldsymbol{e}_2^T\dot{\boldsymbol{e}}_2 \\ &= \boldsymbol{e}_1^T\left(\dot{\boldsymbol{X}}_d - \dot{\boldsymbol{X}}\right) + \boldsymbol{e}_2^T\left(\boldsymbol{G}\boldsymbol{u} + \boldsymbol{f}(X) + \boldsymbol{w}_d - \dot{\boldsymbol{X}}_d - \boldsymbol{k}_1\boldsymbol{e}_1\right) \\ &= \boldsymbol{e}_1^T(-\boldsymbol{e}_2 - \boldsymbol{k}_1\boldsymbol{e}_1) + \boldsymbol{e}_2^T\left(\boldsymbol{G}\boldsymbol{u} + \boldsymbol{f}(X) + \boldsymbol{w}_d - \ddot{\boldsymbol{X}}_d - \boldsymbol{k}_1\dot{\boldsymbol{e}}_1\right) \\ &= -\boldsymbol{e}_1^T\boldsymbol{k}_1\boldsymbol{e}_1 - \boldsymbol{e}_2^T\boldsymbol{k}_2\boldsymbol{e}_2 + \boldsymbol{e}_2^T\tilde{\boldsymbol{w}}_d \\ &= \sum_{i=1}^{6} -k_{1i}e_{1i}^2 - k_{2i}e_{2i}^2 + e_{2i}\tilde{w}_{di}\end{aligned} \tag{33}$$

From Young's inequality, we can obtain that

$$\begin{aligned}\dot{V}_1 &\le \sum_{i=1}^{6} -k_{1i}e_{1i}^2 - k_{2i}e_{2i}^2 + \frac{1}{2}e_{2i}^2 + \frac{1}{2}\tilde{w}_{di}^2 \\ &\le \sum_{i=1}^{6} -k_{1i}e_{1i}^2 - \left(k_{2i} - \frac{1}{2}\right)e_{2i}^2 + \frac{1}{2}\left\|\tilde{\boldsymbol{w}}_d\right\|^2\end{aligned} \tag{34}$$

Let $\kappa = \min\left\{k_{1i}, k_{2i} - \frac{1}{2}\right\}$, we can rewrite (34) as

$$\dot{V}_1 \le -2\kappa V_1 + \frac{1}{2}M_\chi^2 \tag{35}$$

From Lemma 1, we can obtain the solution of (35) as

$$\begin{aligned}V_1(t) &\le e^{-2\kappa(t-t_0)}V_1(t_0) + \frac{1}{2}M_\chi^2 e^{-2\kappa t}\int_{t_0}^{t} e^{2\kappa\ell}d\ell \\ &= e^{-2\kappa(t-t_0)}V_1(t_0) + \frac{M_\chi^2 e^{-2\kappa t}}{4\kappa}\left(e^{2\kappa t} - e^{2\kappa t_0}\right) \\ &= e^{-2\kappa(t-t_0)}V_1(t_0) + \frac{M_\chi^2}{4\kappa}\left(1 - e^{-2\kappa(t-t_0)}\right)\end{aligned} \tag{36}$$

From the above analyses, we can obtain

$$\lim_{t\to\infty} V_1(t) \le \frac{M_\chi^2}{4\kappa} \tag{37}$$

which indicates that $V_1(t)$ is convergent, and the trajectory tracking errors are bounded. More specifically, a superior disturbance observation capability of the LESO contributes better trajectory tracking performances, but with the large observer gains being employed.

### C. ADAPTIVE SWITCHING FUNCTION COMPENSATOR

It is noted that the observation errors of the LESO are bounded, and there is a trade-off between the control gains and the tracking performances. The larger observer gains will decrease the bounded observation errors, but at the cost of a degradation of the system stability. Therefore, further improvements on the tracking accuracy with moderate control gains are needed. Here, an adaptive law is employed to estimate the bounded observation errors of the LESO, based on which a switching function is introduced to compensate for the observation errors of the disturbance observer. Therefore, the requirement of large control gains in the LESO is relaxed, and high gain behavior of the LESO can be avoided.

Define $\boldsymbol{\varpi} = [\varpi_1, \varpi_2, \ldots, \varpi_6]^T \in \Re^6$ as the upper bound of the observation errors $\tilde{\boldsymbol{w}}_d$ generated by the LESO, expressed as follows

$$|\tilde{w}_{di}| \le \varpi_i, \quad i = 1, 2, \ldots, 6. \tag{38}$$

To compensate for the observation errors $\tilde{\boldsymbol{w}}_d$ and further improve the system robustness, a switching function based adaptive compensator is designed as

$$\boldsymbol{u}_{ac} = -\hat{\boldsymbol{\varpi}}\,sign(\boldsymbol{e}_2) \tag{39}$$

where, $sign(\boldsymbol{e}_2) = diag[sign(e_{21}), sign(e_{22}), \ldots, sign(e_{26})] \in \Re^{6\times6}$ denotes the diagonal matrix of the switching functions to compensate for observation errors of the LESO, and the term $\hat{\boldsymbol{\varpi}} = [\hat{\varpi}_1, \hat{\varpi}_2, \ldots, \hat{\varpi}_6]^T$ is tuned online by the following adaptive control law

$$\dot{\hat{\varpi}}_i = \gamma_i\left|e_{2i}\right|, \quad i = 1, 2, \ldots, 6. \tag{40}$$

to estimate the bound $\boldsymbol{\varpi}$. $\gamma_i \in \Re^+$ is the control parameter of the adaptive compensator.

Based on the analysis above, the hybrid compensators (consisting of the robust $2^{nd}$-order LESO and the adaptive switching function) based control scheme for the hexacopter UAV can be achieved as

$$\boldsymbol{u} = \boldsymbol{G}^{-1}\left(\ddot{\boldsymbol{X}}_d + \boldsymbol{k}_1\dot{\boldsymbol{e}}_1 - \boldsymbol{f}(X) - \hat{\boldsymbol{w}}_d + \boldsymbol{e}_1 - \boldsymbol{k}_2\boldsymbol{e}_2 - \hat{\varpi}\,sign(\boldsymbol{e}_2)\right) \tag{41}$$

### D. STABILITY ANALYSIS OF ROBUST AND ADAPTIVE BACKSTEPPING CONTROL SYSTEM

*Theorem 2:* Consider the dynamic system (7) perturbed by the parameter uncertainties and external disturbances, the proposed integrated backstepping control scheme (41) with the disturbance rejection and the adaptive compensation can ensure that the system outputs of the hexacopter UAV converge asymptotically to the designated flight trajectory.

*Proof:* Define the estimation error of the adaptive tuner (40) as $\tilde{\boldsymbol{\varpi}} = \boldsymbol{\varpi} - \hat{\boldsymbol{\varpi}}$, and choose the following Lyapunov function expressed as

$$V_2 = \frac{1}{2}\boldsymbol{e}_1^T\boldsymbol{e}_1 + \frac{1}{2}\boldsymbol{e}_2^T\boldsymbol{e}_2 + \frac{1}{2}\tilde{\boldsymbol{\varpi}}^T\boldsymbol{\gamma}^{-1}\tilde{\boldsymbol{\varpi}} \tag{42}$$

where $\boldsymbol{\gamma} = \mathrm{diag}[\gamma_1, \gamma_2, \ldots, \gamma_6] \in \Re^+_{6\times6}$ is a diagonal matrix.

Taking the derivative of (42) and combing (18,40,41) yield

$$\begin{aligned}\dot{V}_2 &= \boldsymbol{e}_1^T\dot{\boldsymbol{e}}_1+\boldsymbol{e}_2^T\dot{\boldsymbol{e}}_2+\tilde{\boldsymbol{\varpi}}^T\boldsymbol{\gamma}^{-1}\dot{\tilde{\boldsymbol{\varpi}}}\\ &= \boldsymbol{e}_1^T\left(\dot{\boldsymbol{X}}_d-\dot{\boldsymbol{X}}\right)+\boldsymbol{e}_2^T\left(\boldsymbol{G}\boldsymbol{u}+\boldsymbol{f}\left(X\right)+\boldsymbol{w}_d-\dot{\boldsymbol{X}}_d-\boldsymbol{k}_1\boldsymbol{e}_1\right)\\ &\quad+\tilde{\boldsymbol{\varpi}}^T\boldsymbol{\gamma}^{-1}\dot{\tilde{\boldsymbol{\varpi}}}\\ &= \boldsymbol{e}_1^T\left(-\boldsymbol{e}_2-\boldsymbol{k}_1\boldsymbol{e}_1\right)+\boldsymbol{e}_2^T\left(\boldsymbol{G}\boldsymbol{u}+\boldsymbol{f}\left(X\right)+\boldsymbol{w}_d-\ddot{\boldsymbol{X}}_d-\boldsymbol{k}_1\dot{\boldsymbol{e}}_1\right)\\ &\quad+\tilde{\boldsymbol{\varpi}}^T\boldsymbol{\gamma}^{-1}\dot{\tilde{\boldsymbol{\varpi}}}\\ &= -\boldsymbol{e}_1^T\boldsymbol{k}_1\boldsymbol{e}_1-\boldsymbol{e}_2^T\boldsymbol{k}_2\boldsymbol{e}_2+\boldsymbol{e}_2^T\tilde{\boldsymbol{w}}_d-\boldsymbol{e}_2^T\hat{\boldsymbol{\varpi}}sign\left(\boldsymbol{e}_2\right)\\ &\quad-\left(\boldsymbol{\varpi}-\hat{\boldsymbol{\varpi}}\right)^T\boldsymbol{\gamma}^{-1}\dot{\tilde{\boldsymbol{\varpi}}}\\ &= \sum_{i=1}^{6}-k_{1i}e_{1i}^2-k_{2i}e_{2i}^2+e_{2i}\tilde{w}_{di}-\hat{\varpi}_i\left|e_{2i}\right|-\varpi_i\left|e_{2i}\right|\\ &\quad+\hat{\varpi}_i\left|e_{2i}\right|\\ &\leq \sum_{i=1}^{6}-k_{1i}e_{1i}^2-k_{2i}e_{2i}^2-\left(\varpi_i-\left|\tilde{w}_{di}\right|\right)\left|e_{2i}\right|\leq 0\end{aligned}\tag{43}$$

Therefore, $V_2\left(t\right)\leq V_2\left(0\right)$ can be obtained, which indicates that $e_{1i}$ and $e_{2i}$ are bounded. Define function as

$$W\left(t\right)=\sum_{i=1}^{6}k_{1i}e_{1i}^2+k_{2i}e_{2i}^2+\left(\varpi_i-\left|\tilde{w}_{di}\right|\right)\left|e_{2i}\right|\leq-\dot{V}_2\left(t\right)\tag{44}$$

From the mathematical theory, we can obtain that $e_{1i}(t)$ and $e_{2i}(t)$ are uniformly continuous. Therefore, $W(t)$ is also uniformly continuous. Integrating (44) on both sides yields

$$\int_0^t W\left(\tau\right)d\tau\leq V_2\left(0\right)-V_2\left(t\right)\tag{45}$$

Since $V_2\left(0\right)$ is bounded, and $V_2\left(t\right)$ is non-increasing and bounded, the following result can be achieved

$$\int_0^t W\left(\tau\right)d\tau\leq\infty\tag{46}$$

Using the Barbalat Lemma [70], [71], we can obtain $\lim_{t\to\infty}W\left(t\right)=0$, i.e., $\lim_{t\to\infty}e_{1i}\left(t\right)=0$, $\lim_{t\to\infty}e_{2i}\left(t\right)=0$, $\lim_{t\to\infty}\tilde{\varpi}_i\left(t\right)=0$ which indicates that the proposed control scheme can ensure the hexacopter UAV the asymptotical convergence of the system outputs to the designated flight trajectory, even when the parameter uncertainties and external disturbances occur. This completes the proof.

## IV. RESULTS AND DISCUSSION

In this section, to demonstrate the performance and superiority of the proposed control scheme in achieving high-precision tracking, enhanced anti-disturbance capability and feasible control inputs, trajectory tracking flight tests of the hexacopter UAV are carried out in the simulation environment, where parameter uncertainties and external disturbances are introduced. Comparative flight controllers are employed for the trajectory tracking control of the hexacopter UAV system. The performances of system outputs and control inputs are contrastively presented to validate the efficiency and superiority of the proposed controller. The physical and control parameters of the hexacopter UAV system are listed in Tables 1 [72] and 2, respectively.

**TABLE 1. Parameters of the hexacopter UAV.**

| Symbol | Quantity | Value |
|---|---|---|
| $m$ | mass of the body | 1.5 kg |
| $l$ | length of the arm | 0.275 m |
| $g$ | gravitational acceleration | 9.81 m/s$^2$ |
| $I_x$ | moment of inertia around $x$-axis | $3.259\times10^{-2}$ kg· m$^2$ |
| $I_y$ | moment of inertia around $y$-axis | $3.259\times10^{-2}$ kg· m$^2$ |
| $I_z$ | moment of inertia around $z$-axis | $6.059\times10^{-2}$ kg· m$^2$ |
| $K_p$ | thrust coefficient | $1.131\times10^{-5}$ Ns$^2$ |
| $C_d$ | drag coefficient | $1.523\times10^{-7}$ Nms$^2$ |
| $J_r$ | propeller inertia coefficient | $9.90\times10^{-5}$ kg· m$^2$ |

**TABLE 2. Parameters of the proposed controller.**

| Symbol | Quantity | Value |
|---|---|---|
| $\boldsymbol{k}_1$ | Control gains in the | $diag$(2,2,2,5,5,5) |
| $\boldsymbol{k}_2$ | main controller (21) | $diag$(2,2,2,3,3,3) |
| $\boldsymbol{l}_{o1}$ | Control gains in the | $diag$(3,3,3,5,5,5) |
| $\boldsymbol{l}_{o2}$ | | $diag$(1,1,1,1,1,1) |
| $\rho$ | robust compensator (28) | 0.2 |
| $\boldsymbol{\gamma}$ | Control gains in the adaptive compensator (39) | $diag$(2,2,2,2,2,2) |

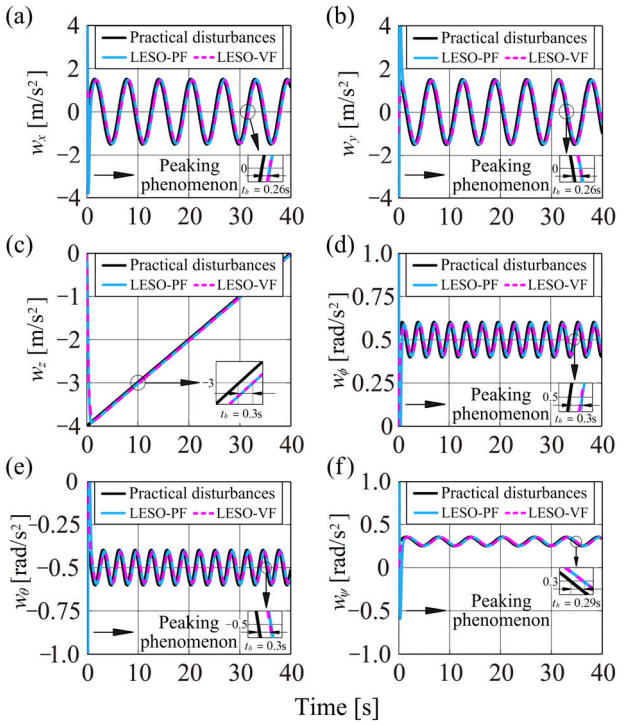


**FIGURE 3. Comparative performances of the LESOs in estimating the whole disturbances perturbing the hexacopter UAV.**

In order to demonstrate the flight performances, perturbed by the parameter uncertainties and external disturbances (shown in Fig. 3), the hexacopter UAV is commanded to track along the reference trajectory made up of the spatial segment polyline, as is shown in Fig. 4. The initial state

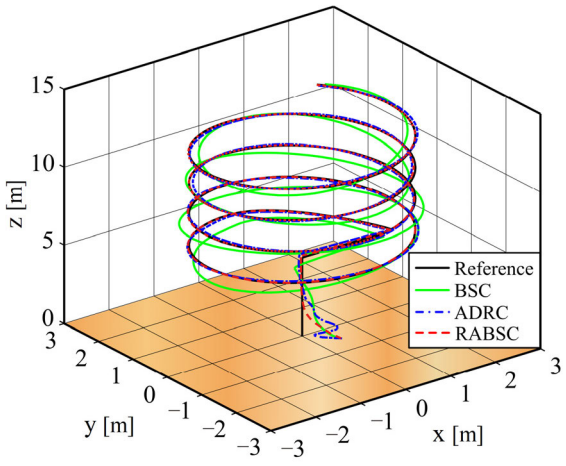


**FIGURE 4.** 3-D trajectory tracking under different control strategies.

condition of the hexacopter UAV system is set as $X_0 = [x_0, y_0, z_0, \phi_0, \theta_0, \psi_0]^T = [0.5, -0.5, 0, 0.1, -0.1, 0.1]^T$.

*Remark 4:* The proper selection of the control parameters in the hexacopter system affects the tracking precision and the control inputs, and there is a trade-off between them. An increase of the control gains $\boldsymbol{k}_{1-2}$ in the main controller contributes higher tracking accuracy, but overshoots of the control inputs may occur. To avoid high gain behaviors of the observer, relative smaller observer gains $\boldsymbol{L}$ are selected. By increasing control gains $\gamma$ in the adaptive compensator, robust tracking performances will be enhanced, but the amplitude of control inputs increases. Note that the attitude control is prerequisite for the trajectory tracking because of the system under-actuation, larger control gains of the attitude subsystem are generally selected than those of the positional one. Overall, control parameters are adjusted until no significant improvements in the tracking performances can be seen.

### A. PERFORMANCE COMPARISON OF 2ND-ORDER AND 3RD-ORDER LESOs

The performances of the $2^{nd}$-order and $3^{rd}$-order LESOs in estimating parameter uncertainties and external disturbances perturbing the hexacopter UAV system are comparatively demonstrated in this subsection. The aerodynamic drag and wind perturbations acting on the translational subsystem are set as a series of sine and cosine functions, and the altitudinal z motion undergoes external load changes, as is shown in Fig. 3(a-c). The rotational subsystem is mainly subjected to model uncertainties, such as the asymmetric structure and rotor fluctuations, as is shown in Fig. 3(d-f). The practical whole disturbances $\boldsymbol{w}_d$ can be expressed as

$$\boldsymbol{w}_P \begin{cases} w_x = 1.5\sin t \\ w_y = 1.5\cos t \\ w_z = -4 + 0.1t \end{cases}, \quad \boldsymbol{w}_\Theta \begin{cases} w_\phi = 0.5 + 0.1\sin(2t) \\ w_\theta = -0.5 + 0.1\cos(2t) \\ w_\psi = 0.3 + 0.1\sin \\ (0.5t)\cos(0.5t) \end{cases} \tag{47}$$

Fig. 3 shows the tracking performance of the observer's estimations $\hat{\boldsymbol{w}}_d$ to their real disturbance values $\boldsymbol{w}_d$. To avoid the high gain behaviors of the LESOs, the moderate observer gains rather than the large ones are selected, which results that the observations lag behind the real disturbances about 0.26-0.30 s. Besides, peaking phenomena exist in the observations of the $3^{rd}$-order LESO due to the initial errors between real position states and initial values in the observer, while that of the $2^{nd}$-order LESO can be avoided owing to zero-initial velocity errors. Therefore, the $2^{nd}$-order LESO with velocity feedback (LESO-VF) has a better observation capability than the $3^{rd}$-order LESO with position feedback (LESO-PF).

*Remark 5:* Without loss of generality, all the initial states of the $2^{nd}$-order and $3^{rd}$-order LESOs are set to be zero. But in practice, the initial positions of the hexacopter dynamics are always different, while the initial velocities are zero at the beginning of the flight. The peaking phenomena in the observation of the $3^{rd}$-order LESO are induced by the initial position errors, and that of the $2^{nd}$-order LESO can be avoided, as is shown in Fig. 3. It is noted that there is not peaking phenomenon in the observation of disturbances in channel-$z$ because the initial $z$-position is equal to that of the observer, i.e. the initial error is zero. Besides, the position information is commonly obtained through integrating the velocity for time, and the integration error will degrade observation performances. The velocity information is more accurate and reliable. Therefore, the $2^{nd}$-order LESO based on the velocity feedback is likely to be more practical than the $3^{rd}$-order one with the position feedback.

### B. PERFORMANCE COMPARISON OF THE DIFFERENT FLIGHT CONTROLLERS

For the sake of comparison study, three flight controllers, i.e., the backstepping controller (BSC) [36], the active disturbance rejection control (ADRC) [63], and the proposed robust and adaptive backstepping control (RABSC) (41) are contrastively investigated and applied in the trajectory tracking control.

Perturbed by the parameter uncertainties and external disturbances exhibited in Fig. 3, the trajectory tracking performances of the hexacopter UAV under the different controllers are contrastively demonstrated, as shown in Figs. 4 and 5. It is shown that the BSC is unable to stabilize the perturbed hexacopter system, while the ADRC with the $3^{rd}$-order LESO ensure the hexacopter UAV satisfactory tracking performance along the reference trajectory, but experiences chattering caused by the peaking phenomena in the initial stage. Also, the proposed control approach achieves an enhanced robust flight capability with higher precision trajectory tracking, owing to the cooperative efforts of the robust and adaptive compensators in estimating and compensating the disturbances. The performance indices RMSE (root-mean-square error) of flight controllers in the trajectory tracking are quantitatively summarized in Table 3.

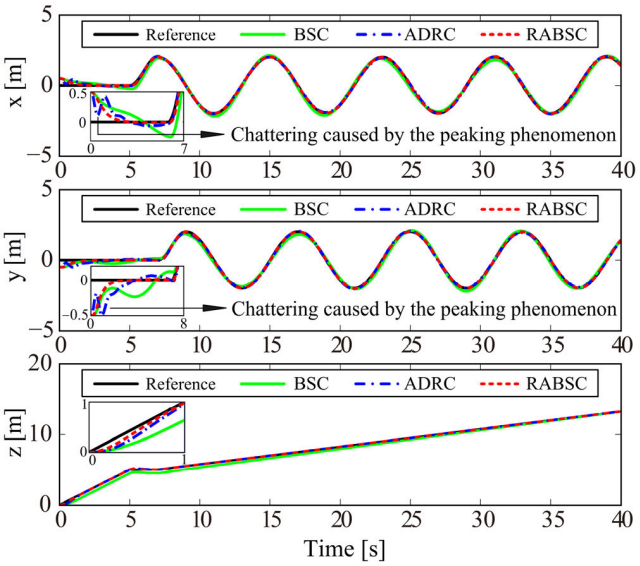


**FIGURE 5.** Comparative performances in positional trajectory tracking under different control strategies.

**TABLE 3.** The output performance indices under different controllers.

| Method | RMSE of x [m] | RMSE of y [m] | RMSE of z [m] |
|---|---|---|---|
| BSC | 0.1790 | 0.1723 | 0.3388 |
| ADRC | 0.1546 | 0.1683 | 0.0584 |
| RABSC | 0.0671 | 0.0697 | 0.0219 |

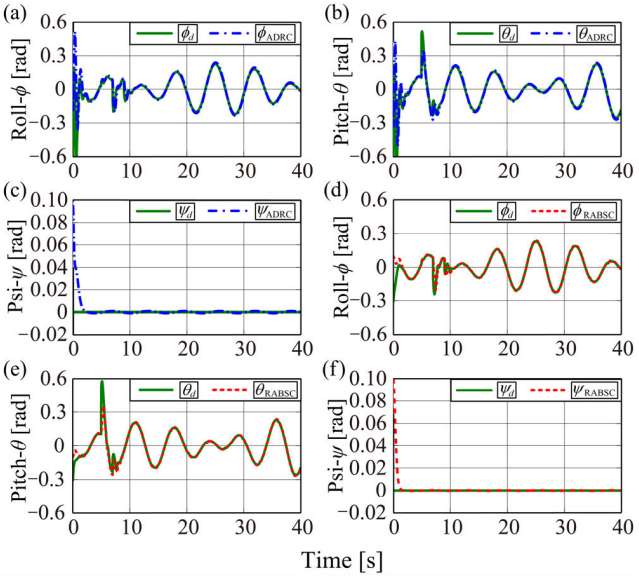


**FIGURE 6.** Comparative performances in positional trajectory tracking under different control strategies.

The corresponding control inputs are comparatively depicted in Figs. 6-8. In terms of the carrying capacity and working efficiency of the actuators, limitations on domains of control signals are set as $u_1 : [0, 33.4]N$, $u_2 : [-3, 3]N \cdot m$, $u_3 : [-2.6, 2.6]N \cdot m$ and $u_4 : [-0.22, 0.22]N \cdot m$ respectively. It can be seen that ADRC can promise the

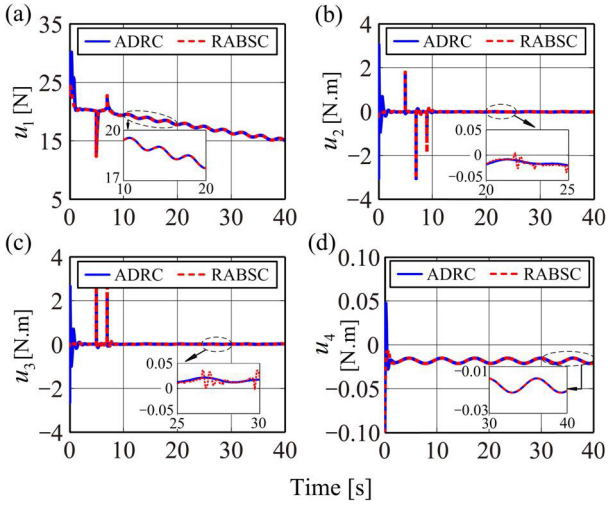


**FIGURE 7.** The contrast of control inputs generated by ADRC and the proposed control scheme.

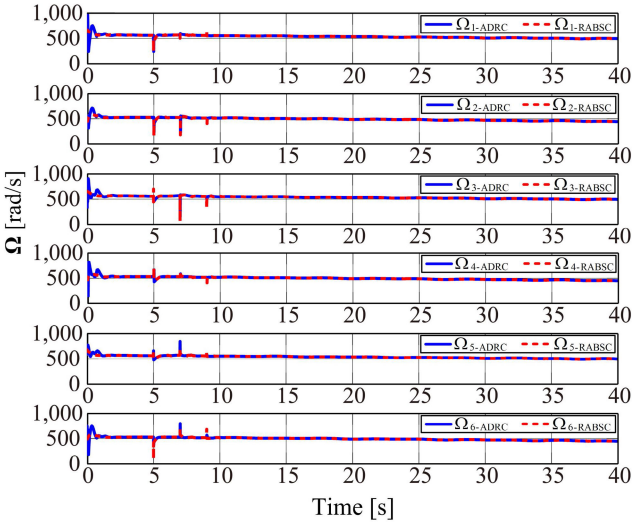


**FIGURE 8.** The contrast of propeller rotation speed under ADRC and the proposed control scheme.

vehicle a robust flight capability, but experiences oscillating attitudes and results in serious chattering inputs in the beginning stage, as is shown in Fig. 6(a-c), Figs. 7 and 8 respectively. The undesired chattering control inputs will consume the limited energy, wear the integrated mechanism, and activate unstable dynamics. Contrastively, the proposed controller has achieved an enhanced robust performance with feasible control inputs being promised, even though some minor chattering occurred. The input performance indices ISCS (integral of squared of control signal: sum [$u_{1-4}$(n) ^2]/n) of robust controllers are quantitatively summarized in Table 4. These demonstrate the efficiency and superiority of the proposed control scheme in the enhanced robustness and feasible control inputs acquisition.

*Remark 6:* The ESO adopted in ADRC is developed based on the position feedback, and peaking phenomena induce serious chattering in control inputs, as is shown in Fig. 7.

**TABLE 4. The input performance indices under robust controllers.**

| Method | ISCS of $u_1$ | ISCS of $u_2$ | ISCS of $u_3$ | ISCS of $u_4$ |
|---|---|---|---|---|
| ADRC | 329.17 | 0.0343 | 0.0319 | 4.1263e-04 |
| RABSC | 326.61 | 0.0043 | 0.0055 | 3.5610e-04 |

In contrast, the proposed control scheme employs a $2^{nd}$-order LESO with velocity feedback, peaking phenomena can be avoided. A modified switching gain $\dot{\hat{\varpi}}_i = \gamma_i(|e_{2i}| - \delta\hat{\varpi}_i)$ and a saturation function are adopted in the adaptive compensator, which is further introduced to compensate for the observation errors $\tilde{\boldsymbol{w}}_d$ rather than whole disturbances $\boldsymbol{w}_d$, only minor chattering exists in the control inputs due to the under-actuation property of the hexacopter UAV.

## V. CONCLUSION AND FUTURE WORKS

In this paper, the nonlinear robust and adaptive backstepping control scheme is hierarchically developed for the robust trajectory tracking control of the hexacopter UAV system. Considering the under-actuated and coupled properties of the hexacopter system, the nominal backstepping controller is firstly employed as the main controller to achieve the fundamental flight performance. By integrating the robust and adaptive compensators with the backstepping based main controller, the proposed control scheme enhances the robustness of the hexacopter system against the disturbances. More specifically, the $2^{nd}$-order linear extended state observer (LESO) based robust compensator with moderate observer gains is introduced to estimate the parameter uncertainties and external disturbances, and the effect of which is restrained to some extent. Also, the adaptive switching function based compensator is cooperatively designed to compensate for the observation errors, through which high gain behaviors of the LESO can be avoided, and robustness of the control system against instabilities has been greatly improved. The Lyapunov analysis is used to ensure the trajectory tracking errors of the hexacopter UAV system asymptotically converge to zero. Comparative simulations under different controllers are carried out to demonstrate the efficiency and superiority of the proposed control scheme in the enhanced robust capability. The future works will concentrate on the investigation of the finite-time stability of control systems, and experiments will be conducted on the real hexacopter UAV to verify the feasibility of the presented control strategy.

## ACKNOWLEDGMENT

The authors would like to thank the reviewers and editors a lot for their precious comments and professional suggestions that helped to improve the paper significantly.

## REFERENCES

[1] N. A. Vu, D. K. Dang, and T. Le Dinh, "Electric propulsion system sizing methodology for an agriculture multicopter," *Aerosp. Sci. Technol.*, vol. 90, pp. 314–326, Jul. 2019.

[2] Y. Chen, G. Zhang, Y. Zhuang, and H. Hu, "Autonomous flight control for multi-rotor UAVs flying at low altitude," *IEEE Access*, vol. 7, pp. 42614–42625, May 2019.

[3] R. Mahony, V. Kumar, and P. Corke, "Multirotor aerial vehicles: Modeling, estimation, and control of quadrotor," *IEEE Robot. Autom. Mag.*, vol. 19, no. 3, pp. 20–32, Sep. 2012.

[4] H. Liu, J. Xi, and Y. Zhong, "Robust attitude stabilization for nonlinear quadrotor systems with uncertainties and delays," *IEEE Trans. Ind. Electron.*, vol. 64, no. 7, pp. 5585–5594, Jul. 2017.

[5] D. Cabecinhas, R. Cunha, and C. Silvestre, "A trajectory tracking control law for a quadrotor with slung load," *Automatica*, vol. 106, pp. 384–389, Aug. 2019.

[6] N. P. Nguyen, W. Kim, and J. Moon, "Super-twisting observer-based sliding mode control with fuzzy variable gains and its applications to fully-actuated hexarotors," *J. Franklin Inst.*, vol. 356, no. 8, pp. 4270–4303, May 2019.

[7] N. Belmonte, S. Staulo, S. Fiorot, C. Luetto, P. Rizzi, and M. Baricco, "Fuel cell powered octocopter for inspection of mobile cranes: Design, cost analysis and environmental impacts," *Appl. Energy*, vol. 215, no. 1, pp. 556–565, Apr. 2018.

[8] R. Ali, Y. Peng, M. T. Iqbal, R. Ul Amin, O. Zahid, and O. I. Khan, "Adaptive backstepping sliding mode control of coaxial octorotor unmanned aerial vehicle," *IEEE Access*, vol. 7, pp. 27526–27534, 2019.

[9] A. Alaimo, V. Artale, C. Milazzo, A. Ricciardello, and L. Trefiletti, "Mathematical modeling and control of a hexacopter," in *Proc. IEEE Int. Conf. Unmanned Aircr. Syst. (ICUAS)*, Atlanta, GA, USA, May 2013, pp. 1043–1050.

[10] B. Tian, H. Lu, Q. Zong, Y. Zhang, and Z. Zuo, "Multivariable finite-time output feedback trajectory tracking control of quadrotor helicopters," *Int. J. Robust Nonlinear Control*, vol. 28, no. 1, pp. 281–295, 2018.

[11] M. Emam and A. Fakharian, "Attitude tracking of quadrotor UAV via mixed H2/H∞ controller: An LMI based approach," in *Proc. IEEE Medit. Conf. Control Autom. (MED)*, Athens, Greece, Jun. 2016, pp. 390–395.

[12] M. Moussid, A. Sayouti, and H. Medromi, "Dynamic modeling and control of a hexarotor using linear and nonlinear methods," *Int. J. Appl. Inf. Syst.*, vol. 9, no. 5, pp. 9–17, 2015.

[13] G. Zhang and H. Taha, "Adaptive back-stepping control applied on octocopter under recoil disturbance," *J. Eng. Sci. Mil. Technol.*, vol. 1, no. 1, pp. 12–21, 2017.

[14] A. Alaimo, V. Artale, C. L. R. Milazzo, and A. Ricciardello, "PID controller applied to hexacopter flight," *J. Intell. Robot. Syst.*, vol. 73, nos. 1–4, pp. 261–270, Jan. 2014.

[15] N. D. Salim, D. Derawi, S. S. Abdullah, S. A. Mazlan, and H. Zamzuri, "PID plus LQR attitude control for hexarotor MAV in indoor environments," in *Proc. IEEE Int. Conf. Ind. Technol. (ICIT)*, Busan, South Korea, Feb./Mar. 2014, pp. 85–90.

[16] O. Araar and N. Aouf, "Full linear control of a quadrotor UAV, LQ vs H∞," in *Proc. IEEE UKACC Int. Conf. Control*, Loughborough, U.K., Jul. 2014, pp. 133–138.

[17] F. Chen, W. Lei, K. Zhang, G. Tao, and B. Jiang, "A novel nonlinear resilient control for a quadrotor UAV via backstepping control and nonlinear disturbance observer," *Nonlinear Dyn.*, vol. 85, no. 2, pp. 1281–1295, 2016.

[18] Q. Wang, H. Zhang, and J. Han, "Research on trajectory planning and tracking of hexa-copter," in *Proc. MATEC Web Conf.*, 2018, pp. 1–6.

[19] Z. Cai, J. Lou, J. Zhao, K. Wu, N. Liu, and Y. X. Wang, "Quadrotor trajectory tracking and obstacle avoidance by chaotic grey wolf optimization-based active disturbance rejection control," *Mech. Syst. Signal Process.*, vol. 128, no. 1, pp. 636–654, Aug. 2019.

[20] R. Analia, Susanto, and K.-T. Song, "Fuzzy+PID attitude control of a coaxial octocopter," in *Proc. IEEE Int. Conf. Ind. Technol. (ICIT)*, Mar. 2016, pp. 1494–1499.

[21] C. Rosales, C. M. Soria, and F. G. Rossomando, "Identification and adaptive PID Control of a hexacopter UAV based on neural networks," *Int. J. Adapt. Control Signal Process.*, vol. 33, no. 1, pp. 74–91, Jan. 2019.

[22] Y. Wang, J. Sun, H. He, and C. Sun, "Deterministic policy gradient with integral compensator for robust quadrotor control," *IEEE Trans. Syst., Man, Cybern., Syst.*, to be published, doi: 10.1109/TSMC.2018.2884725.

[23] J. Liu and X. Wang, *Advanced Sliding Mode Control for Mechanical Systems*. Berlin, Germany: Springer, 2012.

[24] B. Zhao, Y. Tang, C. Wu, and W. Du, "Vision-based tracking control of quadrotor with backstepping sliding mode control," *IEEE Access*, vol. 6, pp. 72439–72448, 2018.

[25] B. Sumantr, N. Uchiyama, and S. Sano, "Least square based sliding mode control for a quad-rotor helicopter and energy saving by chattering reduction," *Mech. Syst. Signal Process.*, vols. 66–67, pp. 769–784, Jan. 2016.

[26] E.-H. Zhang, J.-J. Xiong, and J.-L. Luo, "Second order sliding mode control for a quadrotor UAV," *ISA Trans.*, vol. 53, no. 4, pp. 1350–1356, Jul. 2014.

[27] F. Muñoz, E. S. Espinoza, I. González-Hernández, S. Salazar, and R. Lozano, "Robust trajectory tracking for unmanned aircraft systems using a nonsingular terminal modified super-twisting sliding mode controller," *J. Intell. Robot. Syst.*, vol. 93, nos. 1–2, pp. 55–72, Feb. 2019.

[28] B. Barikbin and A. Fakharian, "Trajectory tracking for quadrotor UAV transporting cable-suspended payload in wind presence," *Trans. Inst. Meas. Control*, vol. 41, no. 5, pp. 1243–1255, Mar. 2019.

[29] F. Santoso, M. A. Garratt, and S. G. Anavatti, "A self-learning TS-fuzzy system based on the C-means clustering technique for controlling the altitude of a hexacopter unmanned aerial vehicle," in *Proc. IEEE Int. Conf. Adv. Mechatronics Intell. Manuf. Ind. Autom. (ICAMIMIA)*, Surabaya, Indonesia, Oct. 2017, pp. 46–51.

[30] T. Dierks and S. Jagannathan, "Output feedback control of a quadrotor UAV using neural networks," *IEEE Trans. Neural Netw.*, vol. 21, no. 1, pp. 50–66, Jan. 2010.

[31] B. Xian, C. Diao, B. Zhao, and Y. Zhang, "Nonlinear robust output feedback tracking control of a quadrotor UAV using quaternion representation," *Nonlinear Dyn.*, vol. 79, no. 4, pp. 2735–2752, Mar. 2015.

[32] R. ul Amin, L. Aijun, M. U. Khan, S. Shamshirband, and A. Kamsin, "An adaptive trajectory tracking control of four rotor hover vehicle using extended normalized radial basis function network," *Mech. Syst. Signal Process.*, vol. 83, no. 15, pp. 53–74, Jan. 2017.

[33] M. Ferdaus, M. Pratama, S. G. Anavatti, and M. Garratt, "A generic self-evolving neuro-fuzzy controller based high-performance hexacopter altitude control system," in *Proc. IEEE Int. Conf. Syst., Man, Cybern.*, Oct. 2018, pp. 2784–2791.

[34] J. Yu, P. Shi, and L. Zhao, "Finite-time command filtered backstepping control for a class of nonlinear systems," *Automatica*, vol. 92, pp. 173–180, Jun. 2018.

[35] T. Madani and A. Benallegue, "Backstepping control for a quadrotor helicopter," in *Proc. IEEE/RSJ Int. Conf. Intell. Robot. Syst.*, Beijing, China, Oct. 2006, pp. 3255–3260.

[36] K. V. Rao and A. T. Mathew, "Dynamic modeling and control of a hexacopter using PID and back stepping controllers," in *Proc. IEEE Int. Conf. Power, Signals, Control Comput. (EPSCICON)*, Thrissur, India, Jan. 2018, pp. 1–7.

[37] B. J. Emran and H. Najjaran, "A review of quadrotor: An underactuated mechanical system," *Annu. Rev. Control*, vol. 46, pp. 165–180, 2018.

[38] J. Qiao, Z. Liu, and Y. Zhang, "Payload dropping control of an unmanned quadrotor helicopter based on backstepping controller," in *Proc. MATEC Web Conf.*, 2019, pp. 1–8.

[39] G. Mester, "Backstepping control for hexa-rotor microcopter," *Acta Technica Corviniensis-Bulletin Eng.*, vol. 8, no. 3, pp. 121–125, 2015.

[40] C. Fu, W. Hong, H. Lu, L. Zhang, X. Guo, and Y. Tian, "Adaptive robust backstepping attitude control for a multi-rotor unmanned aerial vehicle with time-varying output constraints," *Aerosp. Sci. Technol.*, vol. 78, pp. 593–603, Jul. 2018.

[41] T. Jiang, D. Lin, and T. Song, "Finite-time backstepping control for quadrotors with disturbances and input constraints," *IEEE Access*, vol. 6, pp. 62037–62049, 2018.

[42] O. García, P. Ordaz, O.-J. Santos-Sanchez, S. Salazar, and R. Lozano, "Backstepping and robust control for a quadrotor in outdoors environments: An experimental approach," *IEEE Access*, vol. 7, pp. 40636–40648, 2019.

[43] J. Hu, X. Sun, and L. He, "Time-varying formation tracking for multiple UAVs with nonholonomic constraints and input quantization via adaptive backstepping control," *Int. J. Aeronaut. Space Sci.*, vol. 20, no. 3, pp. 710–721, Sep. 2019.

[44] X. Shao, J. Liu, and H. Wang, "Robust back-stepping output feedback trajectory tracking for quadrotors via extended state observer and sigmoid tracking differentiator," *Mech. Syst. Signal Process.*, vol. 104, pp. 631–647, Mar. 2018.

[45] L. Sun and Z. Zheng, "Disturbance-observer-based robust backstepping attitude stabilization of spacecraft under input saturation and measurement uncertainty," *IEEE Trans. Ind. Electron.*, vol. 64, no. 10, pp. 7994–8002, Oct. 2017.

[46] W. Deng, J. Yao, and D. Wei, "Time-varying input delay compensation for nonlinear systems with additive disturbance: An output feedback approach," *Int. J. Robust Nonlinear Control*, vol. 28, no. 1, pp. 31–52, Jan. 2018.

[47] Z.-L. Zhao and B.-Z. Guo, "A novel extended state observer for output tracking of MIMO systems with mismatched uncertainty," *IEEE Trans. Autom. Control*, vol. 63, no. 1, pp. 211–218, Jan. 2018.

[48] C. A. Arellano-Muro, L. F. Luque-Vega, B. Castillo-Toledo, and A. G. Loukianov, "Backstepping control with sliding mode estimation for a hexacopter," in *Proc. IEEE Int. Conf. Electr. Eng. Comput. Sci. Autom. Control*, Mexico City, Mexico, Sep./Oct. 2013, pp. 31–36.

[49] K. Bai, X. Gong, S. Chen, Y. Wang, and Z. Liu, "Sliding mode nonlinear disturbance observer-based adaptive back-stepping control of a humanoid robotic dual manipulator," *Robotica*, vol. 36, no. 11, pp. 1728–1742, Nov. 2018.

[50] C. L. P. Chen, G. X. Wen, Y. J. Liu, and Z. Liu, "Observer-based adaptive backstepping consensus tracking control for high-order nonlinear semi-strict-feedback multiagent systems," *IEEE Trans. Cybern.*, vol. 46, no. 7, pp. 1591–1601, Jul. 2016.

[51] S. Wang, H. Yu, J. Yu, J. Na, and X. Ren, "Neural-network-based adaptive funnel control for servo mechanisms with unknown dead-zone," *IEEE Trans. Cybern.*, to be published.

[52] J. Han, "From PID to active disturbance rejection control," *IEEE Trans. Ind. Electron.*, vol. 56, no. 3, pp. 900–906, Mar. 2009.

[53] Z. Gao, "Scaling and bandwidth-parameterization based controller tuning," in *Proc. IEEE Amer. Control Conf.*, Denver, CO, USA, vol. 6, Jun. 2006, pp. 4989–4996.

[54] X. Shao, J. Liu, H. Cao, C. Shen, and H. Wang, "Robust dynamic surface trajectory tracking control for a quadrotor UAV via extended state observer," *Int. J. Robust Nonlinear Control*, vol. 28, no. 7, pp. 2700–2719, 2018.

[55] Z. Peng and J. Wang, "Output-feedback path-following control of autonomous underwater vehicles based on an extended state observer and projection neural networks," *IEEE Trans. Syst., Man, Cybern., Syst.*, vol. 48, no. 4, pp. 535–544, Apr. 2018.

[56] Z. Chen and J. Huang, "Attitude tracking of rigid spacecraft subject to disturbances of unknown frequencies," *Int. J. Robust Nonlinear Control*, vol. 24, no. 16, pp. 2231–2242, Nov. 2014.

[57] L. Qiao and W. Zhang, "Double-loop integral terminal sliding mode tracking control for UUVs with adaptive dynamic compensation of uncertainties and disturbances," *IEEE J. Ocean. Eng.*, vol. 44, no. 1, pp. 29–53, Jan. 2019.

[58] J. Yao and W. Deng, "Active disturbance rejection adaptive control of hydraulic servo systems," *IEEE Trans. Ind. Electron.*, vol. 64, no. 10, pp. 8023–8032, Oct. 2017.

[59] L. Zhao, L. Dai, Y. Xia, and P. Li, "Attitude control for quadrotors subjected to wind disturbances via active disturbance rejection control and integral sliding mode control," *Mech. Syst. Signal Process.*, vol. 129, pp. 531–545, Aug. 2019.

[60] Z. Zhou, J. Yu, X. Dong, Q. Li, and Z. Ren, "Robust adaptive attitude control of the quad-rotor UAV based on the LQR and NESO technique," in *Proc. IEEE Int. Conf. Control Automat. (ICCA)*, Anchorage, AK, USA, Jun. 2018, pp. 745–750.

[61] X. Wang and B. Shirinzadeh, "Nonlinear augmented observer design and application to quadrotor aircraft," *Nonlinear Dyn.*, vol. 80, no. 3, pp. 1463–1481, May 2015.

[62] C.-C. Hua, K. Wang, J.-N. Chen, and X. You, "Tracking differentiator and extended state observer-based nonsingular fast terminal sliding mode attitude control for a quadrotor," *Nonlinear Dyn.*, vol. 94, no. 1, pp. 343–354, Oct. 2018.

[63] Y. Zhang, Z. Chen, X. Zhang, Q. Sun, and M. Sun, "A novel control scheme for quadrotor UAV based upon active disturbance rejection control," *Aerosp. Sci. Technol.*, vol. 79, pp. 601–609, Aug. 2018.

[64] W. Cai, J. She, M. Wu, and Y. Ohyama, "Disturbance suppression for quadrotor UAV using sliding-mode-observer-based equivalent-input-disturbance approach," *ISA Trans.*, vol. 92, pp. 286–297, Sep. 2019, doi: 10.1016/j.isatra.2019.02.028.

[65] X. Lin, Y. Yu, and C.-Y. Sun, "A decoupling control for quadrotor UAV using dynamic surface control and sliding mode disturbance observer," *Nonlinear Dyn.*, vol. 97, no. 1, pp. 781–795, Jul. 2019.

[66] A. Abadi, A. El Amraoui, H. Mekki, and N. Ramdani, "Guaranteed trajectory tracking control based on interval observer for quadrotors," *Int. J. Control*, to be published, doi: 10.1080/00207179.2019.1610903.

[67] N. Fethalla, M. Saad, H. Michalska, and J. Ghommam, "Robust observer-based dynamic sliding mode controller for a quadrotor UAV," *IEEE Access*, vol. 6, pp. 45846–45859, 2018.
[68] A. Gholami and A. H. D. Markazi, "A new adaptive fuzzy sliding mode observer for a class of MIMO nonlinear systems," *Nonlinear Dyn.*, vol. 70, no. 3, pp. 2095–2105, Nov. 2012.
[69] A. Ioannou and J. Sun, *Robust Adaptive Control*. Upper Saddle River, NJ, USA: Prentice-Hall, 1996.
[70] J.-J. Slotine and W. Li, *Applied Nonlinear Control*. Upper Saddle River, NJ, USA: Prentice-Hall, 1991.
[71] C. Deng and G.-H. Yang, "Distributed adaptive fault-tolerant control approach to cooperative output regulation for linear multi-agent systems," *Automatica*, vol. 103, pp. 62–68, May 2019.
[72] D. Shi, X. Dai, X. Zhang, and Q. Quan, "A practical performance evaluation method for electric multicopters," *IEEE/ASME Trans. Mechatronics*, vol. 22, no. 3, pp. 1337–1348, Jun. 2017.

**JUQIAN ZHANG** received the M.S. degree in mechanical engineering from the School of Mechanical Engineering and Automation, Northeastern University, China, in 2014, where he is currently pursuing the Ph.D. degree in mechanical design and theory. His current research interests include in the fields of aircraft design, nonlinear control system, and flight control for multirotor UAVs.

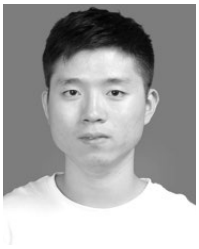

**DAWEI GU** received the M.S. degree in mechanical engineering from the School of Mechanical Engineering and Automation, Northeastern University, China, in 2016, where he is currently pursuing the Ph.D. degree in mechanical design and theory. His current research interests include rotor dynamics, machinery dynamics, and mechanical vibration and control.

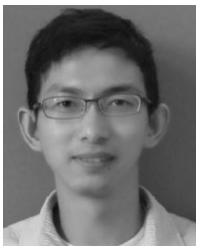

**CHAO DENG** received the Ph.D. degree from Northeastern University, China, in 2018. He is currently a Postdoctoral Research Fellow with the School of Electrical and Electronic Engineering, Nanyang Technological University, Singapore. His research interests include adaptive fuzzy control, cyber–physical systems, cooperative output regulation, and multiagent systems.

**BANGCHUN WEN** received the master's degree from the Department of Mechanical Engineering, Northeast Technology of University (Northeastern University), in 1957.

He is currently a Professor with the School of Mechanical Engineering and Automation, the Honorary Director of Institute of Mechanical Design and Theory, Northeastern University, a member of the Chinese Committee of IFToMM, a member of the Technology Committee of International Rotor Dynamics Committee, a member of the Steering Committee for Asia-Pacific Vibration Committee, the Honorary Chairman of the Chinese Society of Vibration Engineering, and the Honorary Director of the Vibration, Impact, and Noise National Key Lab, Shanghai Jiaotong University. He accomplished many national key research projects, including key projects from the National Fund of Natural Science, 973, 863 projects. He filed ten National patents. He was a recipient of the honor of National Youth and Mid-aged Expert, in 1984. He was also a recipient of two international awards, four National Invention and Science and Technology Progress awards, more than ten Province or Department awards. He was elected to be a member of the Chinese Academy of Sciences. He systematically studied and developed the new course of Vibration Utilization Engineering combined with vibration theory and machinery. In addition, he also studied some problems of rotor dynamics, nonlinear vibration and applications, vibration diagnostics of the machine fault, and the machinery design theories.